

# Nanoscale Horizons

Accepted Manuscript



This is an *Accepted Manuscript*, which has been through the Royal Society of Chemistry peer review process and has been accepted for publication.

*Accepted Manuscripts* are published online shortly after acceptance, before technical editing, formatting and proof reading. Using this free service, authors can make their results available to the community, in citable form, before we publish the edited article. We will replace this *Accepted Manuscript* with the edited and formatted *Advance Article* as soon as it is available.

You can find more information about *Accepted Manuscripts* in the [Information for Authors](#).

Please note that technical editing may introduce minor changes to the text and/or graphics, which may alter content. The journal's standard [Terms & Conditions](#) and the [Ethical guidelines](#) still apply. In no event shall the Royal Society of Chemistry be held responsible for any errors or omissions in this *Accepted Manuscript* or any consequences arising from the use of any information it contains.



[rsc.li/nanoscale-horizons](http://rsc.li/nanoscale-horizons)

## The chiral nano-world: chiroptically active quantum nanostructures

Finn Purcell Milton, † Joseph Govan, † Maria V. Mukhina‡ and Yurii K. Gun'ko†‡\*

†*School of Chemistry and CRANN, University of Dublin, Trinity College, Dublin 2, Ireland*

‡*ITMO University, 197101 St. Petersburg, Russia.*

\*To whom correspondence should be addressed [igounko@tcd.ie](mailto:igounko@tcd.ie)

### Abstract

Chirality is one of the key factors in molecular recognition, therefore the development of new chiral nanoparticles is of great interest to many fields of scientific endeavour including chemistry, biochemistry, pharmacology and medicine. Knowledge of the fundamental concepts relevant to chirality in nanosystems is also very important for further advancement of nanoscience and nanotechnology in general. Over the past years, the use of stereospecific chiral stabilising molecules has opened a new avenue to the area of nanocrystal research. In this review article we present some recent advances in the development of various chiroptically active quantum nanostructures and discuss the latest progress in various approaches for the preparation of these nanostructures. We also consider the intrinsic chirality in quantum nanostructures due to the presence of chiral defects such as screw dislocations and discuss the structure-property relationship. Furthermore, the corresponding potential applications of these chiral nanomaterials has been analysed for key areas: sensing, cytotoxicity mediation and cell imaging, asymmetric catalysis and enantiomeric separation, circular polarised light emitting devices and spintronics. Finally, we provide an outlook for the future development of chiroptically active quantum nanostructures.

### 1. Introduction

Chirality is one of the most fascinating occurrences in the natural world and plays an important role in the fields of chemistry, pharmacology, biology and medicine. A chiral molecule is one that has two mirror-image forms which are non-superimposable in three dimensions. The mirror-image forms of chiral molecules are classified as enantiomers. Chirality is one of the key factors in molecular recognition, which has many uses in

chemistry and biology. Discovering efficient methods to produce and identify enantiopure molecules is critical for the development of pharmaceuticals, agrochemicals, fragrances and food additives and has also been envisaged to play an important role in nanotechnology. Potentially, any nanocrystal can be chiral since they frequently have low symmetry due to the presence of chiral defects in bulk and at the surface.<sup>1</sup> However, nanocrystals in a macroscopic ensemble in solution typically show no optical activity (circular dichroism) for the reason that nanocrystal chirality is random, producing equal portions of the possible enantiomers. Nevertheless, chiral inorganic nanocrystals can be readily designed and fabricated, through a range of approaches. Over the last years the area of chiral metal nanoparticles has received a great deal of attention due to the range of potential applications offered by these materials in chiral sensing, catalysis and as metamaterials in advanced optical devices.<sup>1, 2</sup> The use of stereospecific chiral stabilising molecules has also opened another avenue of interest in the area of quantum dot (QD) research.<sup>3, 4, 5</sup>

Overall, the development of new chiral nanoparticles is of great interest not only for nanotechnology, but also for many other fields of scientific endeavour including chemistry, biochemistry, pharmacology and medicine. In addition, the understanding of the fundamental concepts relevant to chirality in nanosystems is very important for the further advancement of nanoscience and nanotechnology in general. There have been several interesting and useful reviews on a range of chiral nanostructures over the last 3-4 years.<sup>1, 2, 6-9</sup> In this review article we are aiming to present some recent advances in the production, properties and potential applications of various quantum nanostructures.

## 2 Preparation of chiral quantum nanostructures

Over the past few years, the use of stereospecific chiral stabilising molecules has opened an exciting avenue in the area of quantum dot (QD) research. The first chiral QDs (penicillamine stabilised CdS) were prepared by the use of microwave induced heating with the racemic (*Rac*), D- and L-enantiomeric forms of penicillamine as stabilisers.<sup>3</sup> Circular dichroism (CD) studies of these QDs have shown that D- and L-penicillamine stabilised particles produced mirror image CD spectra, while the particles prepared with a *Rac* mixture showed only a very weak signal (Fig. 1A). It was also found that all three types of CdS particles (D-, L-, and *Rac* penicillamine) show very broad emission bands between 400 and 700 nm due to defects or trap states on the surfaces of the nanocrystals (Fig. 1B).

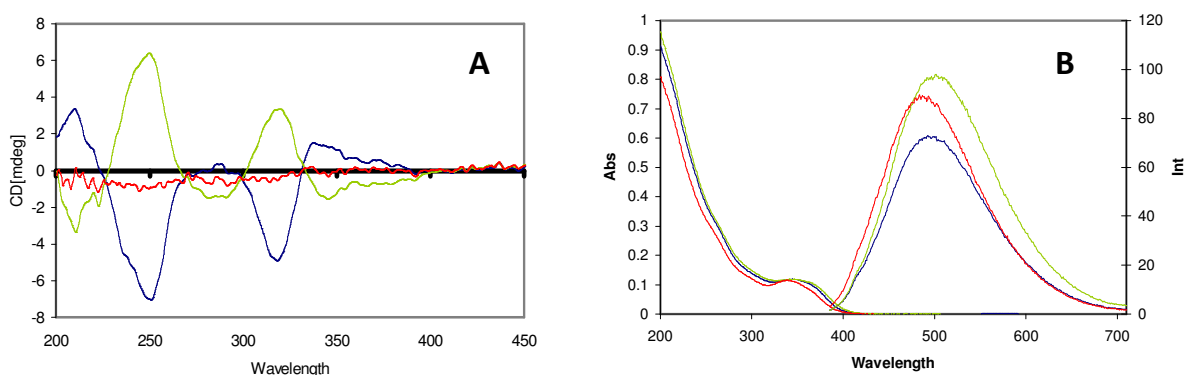


**Fig. 1. A:** CD spectra of D-Pen, (Red), L-Pen, (Green), and *Rac*-Pen, (Blue), modified CdS particles. **B:** UV-Vis (left) and emission spectra (right) of CdS nanocrystals stabilized with D-Pen (Blue), L-Pen (Green), and *Rac*-Pen (Red). Excitation wavelength for all emission spectra is 365nm. Reproduced with permission from reference <sup>3</sup>.

The density functional calculations of these electronic states have demonstrated that longer-wavelength circular dichroism is associated with near-surface cadmium atoms that are enantiomerically distorted by chiral penicillamine ligands, which translate an enantiomeric structure to the surface layers and associated electronic states,<sup>4</sup> while the quantum dot core is found to remain undistorted and achiral. More recently, chiral CdSe QDs<sup>10, 11</sup> CdTe QDs<sup>12, 13</sup> and chiral CdS nanotetrapods (Fig. 2) utilising chiral ligands have been reported.<sup>5, 14</sup> All of these chiral nanostructures also showed a broad distribution of photoluminescence, originating from the emissive defect states and characteristic CD responses within the band-edge region of the spectrum.

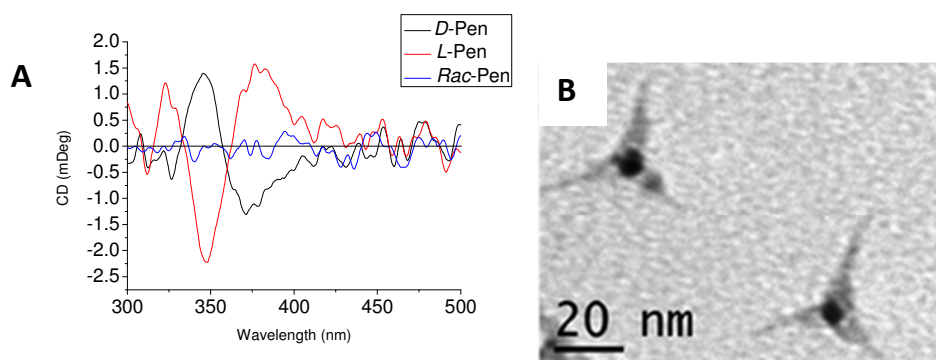


**Fig. 2. A:** CD spectra of penicillamine stabilised CdS tetrapods. **B:** TEM images of D-Penicillamine stabilised nanotetrapods. Reproduced with permission from reference <sup>5</sup>.

The concept of chiral surface defects of QDs (distorted QD shell) was also confirmed by other groups with CdTe nanocrystals bearing chiral D- and L-cysteine-methylester hydrochloride ligands.<sup>15-17</sup> Interestingly, the chirality of the QD surface was maintained even after ligand exchange with an achiral 1-dodecanethiol and transfer of CdTe QDs into a different (organic) phase (Fig. 3). Elemental analyses demonstrated that more than 92% of cysteine-methylester molecules were exchanged with dodecanethiol. In this case, the behaviour of QDs can be explained by the formation of chiral kink structures which are preserved during the ligand-exchange process, resulting in an unusual chiral memory effect.

16

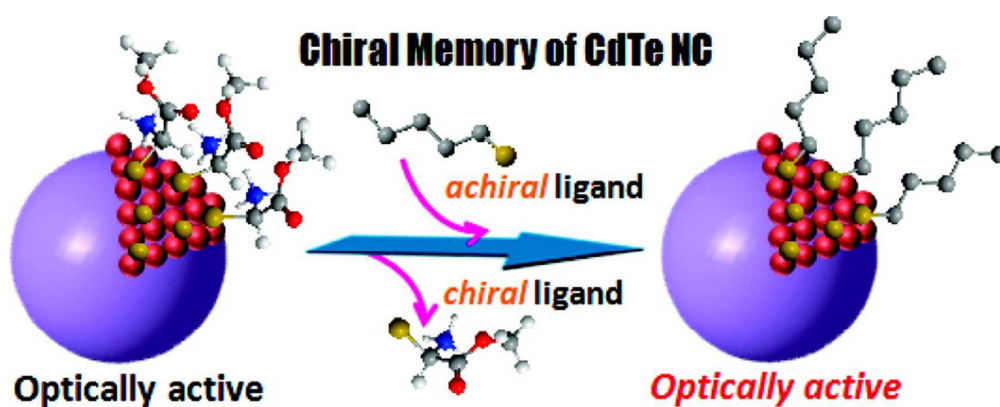


**Fig. 3.** Chiral memory of thiol-capped CdTe nanocrystals. QDs stabilized with chiral ligands retained their optical activity even after exchange with an achiral thiol. Reproduced with permission from reference <sup>16</sup>.

However, chirality in chiral QDs can be caused not necessarily only by chiral surface defects but also by other factors. For example, a remarkable phenomenon of chiral ligand induced circular dichroism in CdSe quantum dots was reported by M. Balaz et al.<sup>18, 19</sup> The researchers have found that chiral thiol capping ligands such as L- and D-cysteine can induce chiroptical properties in originally achiral cadmium selenide quantum dots (CdSe QDs). The preparation involved a simple phase transfer of achiral trioctylphosphine oxide or oleic acid capped CdSe QDs from toluene into aqueous phase using L- and D-cysteine by stirring the mixture at RT in the absence of light for 24 h. It was found that L- or D-cysteine stabilized QDs in aqueous phase demonstrated size-dependent electronic circular dichroism (CD) and circularly polarized luminescence (CPL). As expected, mirror images opposite CD and CPL signals have been shown by CdSe QDs capped with D- and L-cysteine (Fig. 4). In addition, it was found that the CD profile and CD anisotropy varied with size of CdSe nanocrystals with

the largest anisotropy observed for CdSe QDs of 4.4 nm. The authors have also performed time Dependent Density Functional Theory (TDDFT) calculations showing the attachment of L- and D-cysteine to the surface of model  $(\text{CdSe})_{13}$  nanoclusters (NCs) that induces measurable opposite CD signals for the excitonic band of the nanocluster (Fig. 4). It was suggested that such redesign and modulation of chiroptical properties could lead to applications in chiroptical memory, chiral biosensing and chiroptical nanomaterials.

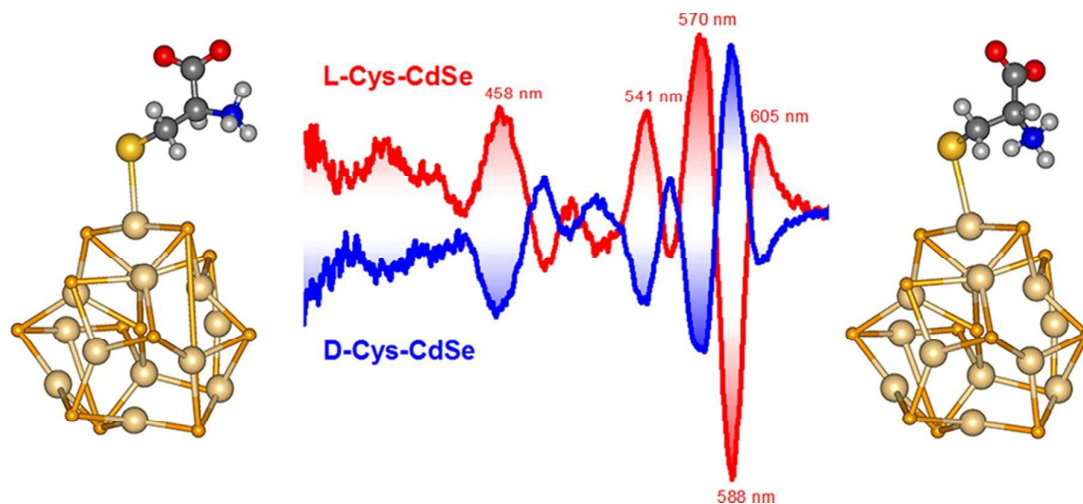


**Fig. 4.** Middle: CD spectra of L-Cys-CdSe (red curves) and D-Cys-CdSe (blue curves) and DFT optimized geometries of (left) L-Cys- $(\text{CdSe})_{13}$  and (right) D-Cys- $(\text{CdSe})_{13}$  NCs. Reproduced with permission from reference <sup>18</sup>.

Interesting effects of cysteine enantiomers on optical isomerism, growth rate and product structure of chiral CdTe based QDs was reported by Kotov et al. <sup>17</sup> This paper postulated that the atomic origin of chiral sites in nanoparticles is geometrically similar to that in organic compounds. Using theoretical calculations and experimental data the researchers demonstrated that the atoms in chiral cysteine stabilised CdTe nanocrystals are arranged as tetrahedrons and chirality occurs when all tetrahedral apexes have chemical differences and substitution. <sup>17</sup> More recently the same group has shown that irradiation of a racemic suspension of CdTe QDs with circularly polarized light leads to the conversion of the QDs into twisted chiral quantum nanoribbons with an enantiomeric excess exceeding 30% (Fig.5). <sup>20</sup> This discovery opens up a new approach to induce chirality and produce novel chiral nanostructures using circular polarised light as a driving force and a “template”.

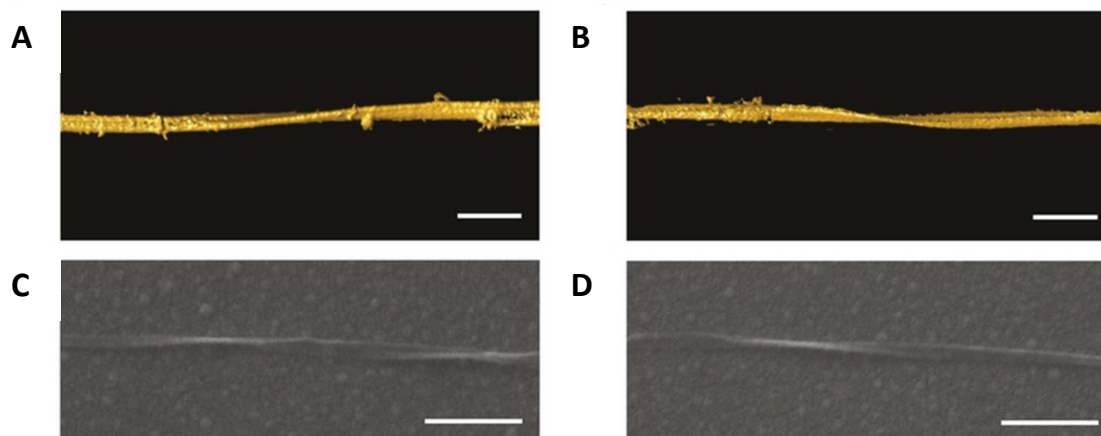


**Fig. 5.** Chirality of single CdTe nanoribbons. **A,B**, Surface rendering of the 3D TEM tomographic reconstruction of a LH (**C**) and a RH (**D**) nanoribbon. Scale bars, 100 nm. Reproduced with permission from reference <sup>20</sup>.

### 3. Intrinsic chirality in quantum nanostructures

In recent times, more attention has been paid to the understanding of the origin of intrinsic chirality in various nanocrystals. It has been shown <sup>21, 22</sup> that as-prepared CdSe QDs form a racemic mixture (D:L=50:50) of left-handed (L) and right-handed (D) enantiomers during standard hot injection synthesis. Optically active ensembles of QDs (Fig. 6) were isolated by extracting either L or D QDs from a racemic sample with chiral cysteine molecules (an organic-aqueous phase transfer approach) that bind with different affinities to the chiral surfaces of the QD enantiomers. After separation, the QDs with lower affinity to chiral ligands (L enantiomers in the case of using L ligands and *vice versa*) were still isolated in the organic phase and capped with achiral ligands, but began displaying circular dichroism (CD). So in this case, the observed CD signals should be attributed to chiral QDs themselves rather than ligand induced optical activity.

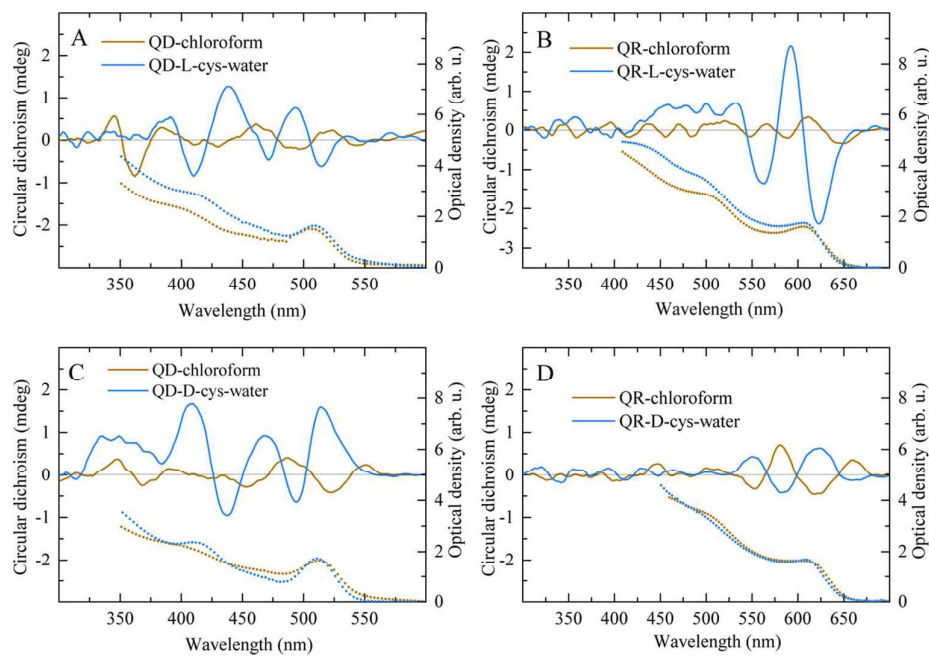


**Fig. 6.** Chiroptical properties of the CdSe/ZnS QD and QR solutions after chiral resolution. The absorption (dotted lines) and CD (solid lines) spectra of the chloroform and aqueous phases of the QDs (A and C) and QRs (B and D) after enantioselective phase transfer with L-cysteine (A and B) and D-cysteine (C and D). Reproduced with permission from reference <sup>21</sup>.

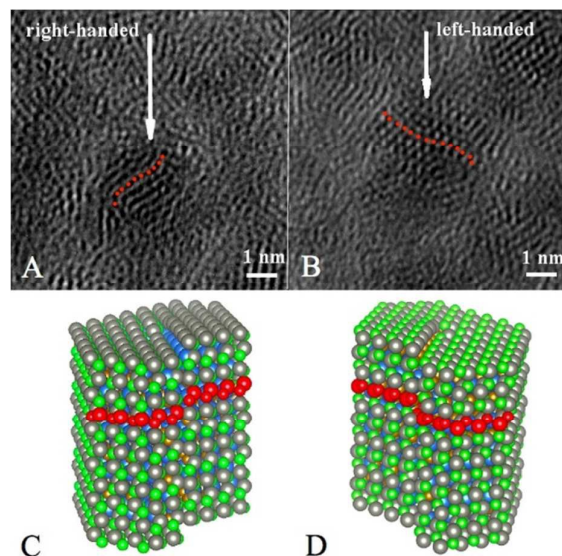


**Fig. 7.** (A, B) TEM images of the CdSe/ZnS QDs. The arrows indicate possible screw dislocations. (C, D) Atomistic models of CdSe/ZnS QDs with right (C) and left (D) screw dislocations. Dislocations are set in the (010) plane of CdSe core of nanocrystals with (-) Burgers vector (C) and (+) Burgers vector (D). Red dotted lines indicate the direction of the dislocations. Reproduced with permission from reference <sup>21</sup>.

Alternatively, the chiral separation can be achieved via an incubation of the CdTe QDs capped with achiral ligands and displayed no CD signal with chiral bovine serum albumin (BSA).<sup>20</sup> After the separation of BSA-containing adsorbate and unbound QDs, the QDs showed a positive CD signal. Using materials with intrinsically chiral crystal lattice such as quartz,  $\beta$  - AgSe,  $\alpha$  - HgS, selenium, and tellurium is another way to prepare intrinsically chiral nanocrystals. It has been shown<sup>23</sup> that the synthesis of  $\alpha$  - HgS nanocrystals produces a CD response an order of magnitude greater than the CD response of chiral nanocrystals with achiral crystal lattices (CdSe, CdS, CdTe). A pump–probe scheme was applied to theoretically investigate CD of intraband transitions and demonstrate that intrinsic optical activity from the achiral wurtzite crystal lattices arises from symmetry breaking induced by the presence of chiral defects (screw dislocations) naturally forming during uniaxial growth of wurtzite nanocrystals (Fig. 7).<sup>24, 25</sup> Also, density functional theory (DFT) calculations of the complexes of L-cysteine molecules and  $Zn_{13}S_{13}$  nanoclusters distorted with right-handed and left-handed screw dislocations has been performed to show that screw dislocations dissymmetrically distort the NC's surfaces causing difference in binding energies for chiral ligands to the oppositely distorted NC's surface, thus enabling enantiomer separation during enantioselective phase transfer.<sup>21</sup>

Semiconductor nanocrystals are not the only example of nanoscale objects with individual intrinsic chirality. Previously, the overall structure of  $Au_{102}$  nanoclusters has been proved to be chiral using high-resolution X-ray diffraction.<sup>26</sup> In further experiments, intrinsic chirality has been demonstrated for  $Au_{38}$  NCs, by firstly identifying its structure through X-ray crystallography,<sup>27</sup> then via separation of the enantiomers achieved by chiral high-performance liquid chromatography,<sup>28</sup> and for  $Au_{102}$  NCs via a chiral phase transfer approach<sup>29</sup> similar to the one used for separation of semiconductor QD enantiomers<sup>21</sup>. In the case of  $Au_{38}$ ,<sup>30</sup>  $Au_{40}$ ,<sup>30</sup>  $Au_{28}$ ,<sup>31</sup> and  $Au_{102}$ <sup>29</sup> nanoclusters, chirality originates from these clusters when protected by thiolate ligands (-SR) and is associated with the chiral SR-Au-SR and 2 SR-(Au-SR)<sub>2</sub> motifs forming the arrangement of achiral ligands on the surface of NC's achiral cores. Recently a giant chiral Au cluster,  $Au_{133}(SR)_{52}$ , was identified using x-ray crystallography, which exhibits multiple origins of chirality, ranging from “swirls” of the ligands' carbon tails, ladder-like helical “stripes” of Au-SR-Au surface motifs to the chiral  $Au_{107}$  core of the structure.<sup>32</sup>

#### 4. Potential applications of chiral quantum nanostructures

Chiral quantum confined nanostructures demonstrate a range of unique properties, making them distinctly fitted to a variety of applications, which can be divided into five distinct areas: (i) sensing, (ii) cytotoxicity mediation and cell imaging, (iii) asymmetric catalysis and enantiomeric separation, (iv) circularly polarised light sources and (v) spintronics.

##### 4.1 Sensing

Quantum dots (QDs) and metal nanoclusters (NCs) have been extensively explored as sensors for a range of different species<sup>33</sup> including, biomolecules<sup>34, 35</sup>, chemicals<sup>36, 37</sup>, light<sup>38</sup>, temperature<sup>39</sup>, and pH<sup>40</sup>. Chiral QDs potentially offer a unique opportunity as sensors for the detection of other chiral systems. One such example of chiral sensing is the use of CdSe/ZnS QDs capped in, either  $\alpha$ - cyclodextrin or  $\beta$ - cyclodextrin in water<sup>41</sup>. These QDs showed the ability to sense the presence of two amino acids, tryptophan (Tyr) and methionine (Met) due to a fluorescence enhancement which was found to be highly enantioselective to the chirality of the amino acid. The fluorescence intensity of  $\beta$ - cyclodextrin QDs increased by 71% from the original intensity when L-Tyr was present ( $5 \times 10^{-5}$  M), but only 8% with D-Tyr ( $5 \times 10^{-5}$  M). Therefore, the net fluorescence intensity increase of  $\beta$ - cyclodextrin -QDs due to L -Tyr is found to be 7.09 times than that of D-Tyr. Treatment of  $\alpha$ - cyclodextrin -QDs with L -Met led to a significant fluorescence enhancement of 51%. In contrast, while the presence of D-Met produced a 15 % increase giving an enantiomeric fluorescence difference ratio of 3.4.

Another example of enantioselective photoluminescence enhancement was demonstrated using mono-6-SH- $\beta$ -cyclodextrin Mn-doped ZnS QDs as an effective sensor for Tyr<sup>42</sup>. These QDs are found to be highly luminescent, showing dual emission peaks, the first at 430 nm due to the crystal defects of ZnS and 590 nm corresponding to the  ${}^4T_1-{}^6A_1$  transition of the Mn dopant. When these QDs interacted with L-Tyr, enhancement of the PL peak at 430 nm along with a blue shift to 399 nm occurred, while little change was found for D-Trp in regards to peak position or intensity. It should also be noted no noticeable effect occurred regarding emission at 590 nm for either enantiomer. Therefore, L-Tryptophan enhanced the PL intensity of  $\beta$ -CD-Mn-ZnS QDs drastically, whereas the D-enantiomer barely affected it. The detection of L-Tyr shows good linearity in the range of 0–6.0  $\mu$ M, with a limit of detection of 5.4 nM. This system has also been shown in an earlier report to be highly selective to only the tryptophan amino acid, with other amino acids showing no substantial effect upon the luminescence of the QDs, even at the high concentration of 50 mM<sup>43</sup>. The stereoselective inclusion and subsequent hydrolysis of Trp enantiomers by  $\beta$ -CD-Mn-ZnS is proposed as the

mechanism for this observed chiral discrimination. Instead of fluorescence enhancement, quenching of fluorescence is a different route to achieve enantioselective recognition and was demonstrated using CdSe/ZnS QDs capped with D or L cysteine, which showed enantiomeric quenching of fluorescence dependent upon the chirality of a dipeptide, carnitine<sup>44</sup>. Upon adding D-carnitine, a dramatic loss of the fluorescence of L-Cys-capped QDs was observed. In contrast, the fluorescence of D-Cys-capped QDs was not affected by the addition of D-carnitine while the enantiomer L-carnitine selectively quenches the fluorescence of D-Cys-capped QDs but not of L-Cys-capped QDs. Chiral selective quenching was also demonstrated in another paper with the use of N-acetyl-L-cysteine methyl ester (L-CysP) capped CdSe/CdS QDs<sup>45</sup>, which showed a significant chiral discrimination of aryl propionic acids enantiomers, particularly for those of ketoprofen, flurbiprofen, and naproxen, all types of non-steroidal anti-inflammatory drug. The fluorescence of the QDs showed concentration and enantiomer dependent quenching, with L-CysP-QDs showing stronger quenching from the R enantiomer rather than the S of the tested drug, with the most pronounced effect seen with ketoprofen.

Another interesting example utilizing L-Cys CdS QDs as sensors for non-chiral metal ions has also been demonstrated, using the resulting change in CD signal of the chiral QDs as a means to determine the presence of a given metal ion<sup>46</sup>. This process proved remarkably sensitive to Ni<sup>2+</sup> and Co<sup>2+</sup> ions, showing little response to a range of other cations. The QDs were also shown to be an effective tool for these metal ions detection in real water analysis compared to the results obtained from ICP-OES. The change in the CD of the QD was determined to be due to metal complex formation between cysteine molecules on the surface of the QD and the ions in solution. A linear relationship between the ratio of luminescence decrease and Ni<sup>2+</sup> or Co<sup>2+</sup> concentration is observed in the range of 20 – 60 mM and 10 – 80 mM for Ni<sup>2+</sup> or Co<sup>2+</sup> respectively. The quenching efficiency was also determined, termed the Stern–Volmer quenching constant, to be  $3.57 \times 10^5 \text{ M}^{-1}$  for Ni<sup>2+</sup> and  $1.00 \times 10^4 \text{ M}^{-1}$  for Co<sup>2+</sup>, which is remarkably high, indicating excellent sensitivity to these ions.

Metal nanoclusters have also demonstrated their applicability to chiral sensing, with Ag NCs of on average 1.5 nm in diameter capped in L- glutathione showing selective quenching when mixed with L- or D- cysteine<sup>47</sup>. Interestingly, in this work, upon the addition of L-Cys, an obvious fluorescence quenching of Ag NCs was observed, however, the fluorescence of Ag NCs was scarcely reduced by the addition of D-cysteine. This test under optimal conditions showed the lower limit of L-Cys detection to be 3.4 mM. The selectivity of this quenching

was also investigated, with no apparent changes in fluorescence when other chiral amino acids and biomolecules (e.g. human serum albumin, bovine serum albumin, uric acid, ascorbic acid and glucose) were added. A final suggestion, which we have not found in the literature to date, would be to utilise the CPL signal of a QD or NC, to detect the presence of a chiral material, which should offer a unique approach to sensing.

An interesting new strategy for nonexclusive fluorescence sensing of enantiomers using chiral nanoparticles and their ability to form dynamic assemblies was offered by Y. Xia et al. (Fig. 8).<sup>48</sup> The researchers have found that fluorescence resonance energy transfer (FRET) in nanoscale assemblies consisting of either L-cysteine- or D-cysteine-modified quantum dots (QDs) and gold nanorods (GNRs) is strongly dependent on traces of enantiomeric cysteine molecules. This phenomenon was explained by the high sensitivity of dynamic QD-GNR assemblies to the weak inter-nanoparticle interactions that can exponentially increase energy transfer efficiencies from QDs to GNRs. Both enantiomers at different concentrations of cysteine have been determined by comprehensive analysis of the data from two nonexclusive sensing platforms. It was shown that this technique enables the quantification of the composition of a chiral sample even if the content of one enantiomer in the mixture is as low as 10%. The authors believe that this methodology may be expanded by designing other sensing systems for chiral assays of drugs, metabolites, and other chemicals.

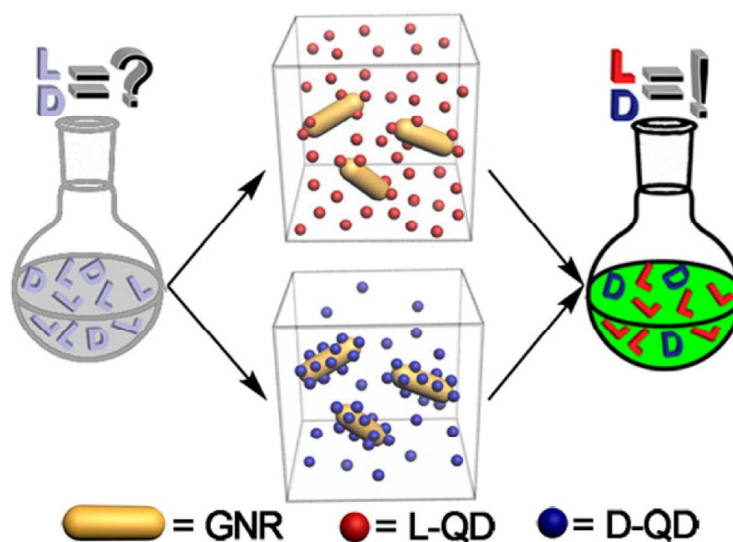


**Fig. 8.** Schematic illustration of nonexclusive QD/GNR based FRET sensors for chiral assays in two individual systems. Reproduced with permission from reference<sup>48</sup>.

In another example; it was reported that CdSe/ZnS nanoparticles capped with N-acetyl-L-cysteine methyl ester can be used for sensing of various chiral organic drug molecules<sup>49</sup> In this case; chiral QDs consisting of an inorganic CdSe/ZnS core-shell and a chiral organic ligand have been prepared by a simple ligand exchange reaction of commercially available amine-capped QDs with methyl ester N-acetyl-L-cysteine. These chiral QDs were then used to perform studies of the chiral recognition of drugs, in particular the aryl propionic acids, ketoprofen, naproxen, flurbiprofen and ibuprofen. It was found that all of the drug molecules quenched the QD emission in a concentration- dependent mode. The spectral differences in the behavior of R- and S enantiomers of these aryl propionic acid drugs enabled a quantitative determination of both chiral forms in mixtures and pharmaceutical samples.

#### 4.2. Cytotoxicity mediation and cell imaging

The effect of nanomaterials upon different biological systems is a vitally important area, with a range of key steps in its understanding having already been made.<sup>50-53</sup> Only recently; the effect of chirality has been analysed in this context. It has been found that in the case of chiral nanostructures, opposite enantiomers can interact quite differently with biological systems, which are homochiral, and therefore the biological toxicity of nanoparticles can be mediated via the chirality of the nanoparticles. For example, a recent study<sup>54</sup> examined the effect, on resulting cytotoxicity of two different sizes of CdTe QDs capped in L or D enantiomers of a tripeptide, glutathione (GSH). This was carried out by comparing the effects of QDs on cell viability in human hepatoma HepG2 cells, which was shown to exhibit concentration- and chirality-dependent cytotoxicity, with L-GSH-QDs showing greater cytotoxicity for a given concentration<sup>54</sup>. The ability of these QDs to induce autophagy was also examined for these cells relative to controls, with all four QDs tested triggering conversion of microtubule-associated protein light chain 3 (LC3)-I to LC3-phosphatidylethanolamine conjugate (LC3-II), an effective marker of autophagy. This activation of autophagy was chirality-dependent, with L-GSH-QDs inducing a more dramatic effect.

The cytotoxicity of small chiral light-emitting metal nanoclusters has also recently been investigated with small L or D - GSH capped Ag NCs (so called “silver quantum dots”)<sup>55</sup> used *in vivo* testing to measure their effect on the human gastric cancer cell line, MGC-803 and human gastric mucous epithelial cell line GES-1. The results showed higher cytotoxicity in D-GSH Ag NCs capped, comparatively to L-GSH Ag NCs for both MGC-803 and GES-1

cells which is shown by the IC<sub>50</sub> (half-maximum inhibitory concentration) values of  $724.88 \pm 35.27$  and  $832.69 \pm 38.87$  mg mL<sup>-1</sup> for L-GSH Ag NCs treated MGC-803 and GES-1 cells while for D-GSH Ag NCs a higher inhibitory effect was found for MGC-803 and GES-1 cells of IC<sub>50</sub> values of  $481.34 \pm 2.26$  and  $598.09 \pm 9.34$  mg mL<sup>-1</sup>, respectively). The MGC-803 cells showed lower cell viability while the GES-1 cells seemed to maintain a better balance between the generation and elimination of reactive oxygen species (ROS) and to exhibit a higher resistance to oxidative stress, leading to a relatively high viability.<sup>55</sup> The principle of the induction of ROS is also used to explain the difference in cytotoxicity measured between the enantiomers Ag NCs.

A similar study was carried out with small chiral Au NCs capped with either L-GSH or D-GSH and their effects upon normal GES-1 cells and cancerous MGC-803 cells. This study showed that both L-GSH-Au NCs and D-GSH-Au NCs could induce dose-dependent cytotoxicity for both MGC-803 and GES-1 cells, and a cell physiology-based toxicity study revealed integrated cytotoxic effects including ROS generation, mitochondrial depolarization, DNA damage, cell cycle arrest, and apoptosis mediated death. This meant that D-GSH-capped Au NCs are evidently more toxic than L-GSH-capped ones for both MGC-803 and GES-1 cells and again demonstrates the role of chirality regulation of cytotoxicity at the nano-level.<sup>56</sup>

Also due to the luminescent properties, high quantum yields, variable absorption and emission wavelength, outstanding photostability and excellent biocompatibility in certain cases, quantum dots or small metal nanoclusters offer a unique option for cell imaging.<sup>57-60</sup> Recently; using a confocal laser scanning microscopy it has been demonstrated that penicillamine (Pen) capped 1-3 nm Au NCs can be taken up by HeLa cells after a 2 h incubation time.<sup>61</sup> The emission intensity of L-Au NCs was depicted in green and the luminescence from the nanoclusters ingested by HeLa cells indicated that L-Au NCs did not distribute effectively in the cells with the majority of the Au NCs found on the cell surface or in the cell. Comparing the resulting confocal images of HeLa cells incubated with L-Au NCs, the emission intensity of HeLa cells incubated with D-Au NCs was stronger which is consistent with the fluorescence quantum yields of L-Au NCs and D-Au NCs in aqueous solution. This was then followed by an investigation of the cytotoxicity of Pen -Au NCs, with cell viabilities upon exposure to these Au NCs. From this study, it was found that L-Au NCs and D-Au NCs showed nearly no cytotoxicity at a concentration of 8 mM compared to DL-Au NCs, which showed high cytotoxicity at this concentration. When the concentrations were increased to 80 mM, L-Au NCs and D-Au NCs showed much higher cytotoxicities.

Interestingly, overall, the cytotoxicities of the homo chiral Pen-Au NCs was much lower than the DL-Pen-Au NCs (Fig. 9).

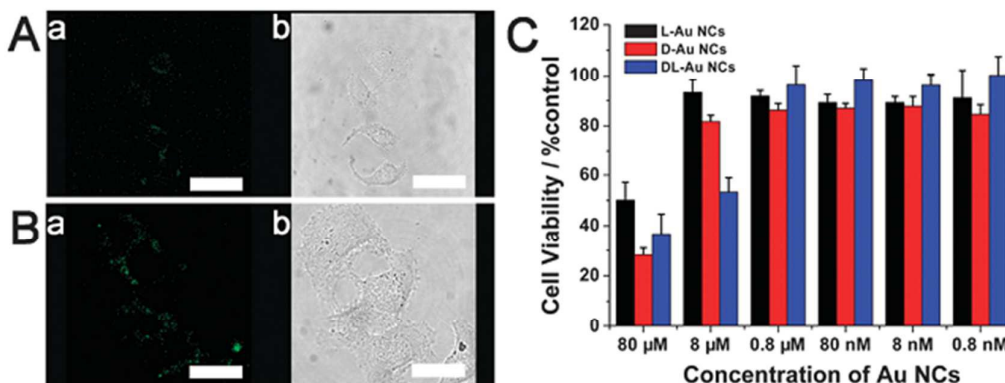


Fig. 9. (A) Confocal image of HeLa cells after incubation with L-Au NCs for 2 h, scale bars: 20 mm. (B) Confocal image of HeLa cells after incubation with D-Au NCs for 2 h, scale bars: 20 mm. (C) Cytotoxicity of the chiral PA protected Au NCs on HeLa cells was measured by MTT assays ( $n = 8$ , mean S.D.), the result showed the relative cell viability of the cells accompanied by silver nanoclusters at the final concentrations of 0.8 nM, 8 nM, 80 nM, 0.8 mM, 8 mM and 80 mM. The viability of the positive control that was treated with the same volume of water was taken as 100%. Reproduced with permission from reference <sup>61</sup>.

#### 4.3. Enantiomeric separation and asymmetric catalysis

Enantiomeric separation is an approach used to separate one chiral enantiomer from another. A range of different approaches exist to achieve this, the majority of which fall under preferred crystallisation <sup>62, 63</sup>, kinetic resolution by enzymes <sup>64</sup> and chromatographic separation <sup>65</sup>, with chromatography being the most practised approach.<sup>66</sup> Lately, an alternative possible example has been presented by homochiral NPs, through the use of the selective binding sites of these chiral nanoparticles, one can enable selective adsorption of one enantiomer over another. This has been demonstrated in a range of nanomaterials and has been recently reviewed <sup>66</sup>. Unfortunately, at present no examples exist of the application of quantum confined materials being used in this role, though they would offer a unique opportunity for application in this area due to the large surface area of these particles and the possible dual function since these particles can serve as enantioselective sensors.

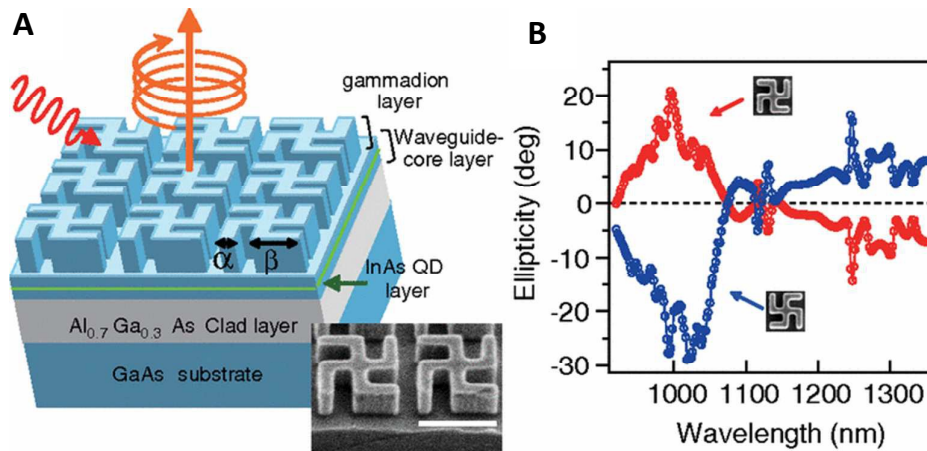
Asymmetric catalysis is an important synthetic tool used in chemistry to favour a specific enantiomer over another, with asymmetric catalytic design proving to be some of the most challenging catalysts to produce. Nanoscience has seen wide application in selective catalysis

<sup>67</sup>, with new examples of asymmetric catalysts being demonstrated using a range of metal nanoparticles (MNP) <sup>68, 69</sup>, metal oxides <sup>70-72</sup>, metal sulphides <sup>73</sup> and SiO<sub>2</sub> <sup>74, 75</sup>. There is also an example of the use of ZnS QDs with an induced chirality as a catalyst for asymmetric aldol condensation reactions.<sup>73</sup> In this case ZnS nanoparticles have been synthesized by a co-precipitation of ZnS in the presence of L-proline. Then these nanoparticles were used as a catalyst for the direct asymmetric aldol reaction of several aldehydes with acetone to achieve chiral  $\beta$ -hydroxy carbonyl compounds in good yield and enantioselectivity at room temperature without using any co-solvent for solubility purposes. It was found that the selectivity of ZnS nanoparticles enables the production of only (R)- $\beta$ -hydroxy carbonyl compounds and restricted the reaction to the aldolization stage only. Importantly the ZnS catalyst was recovered and reused several times without any considerable loss of activity. Therefore chiral quantum confined nanomaterials have found only very limited applications in asymmetric catalysis to date. However; these materials presents great potential opportunities as catalysts in asymmetric photocatalysis, due to their tuneable absorption and unique energy transfer properties.

#### 4.4. Circularly polarised light sources

Another emerging application of luminescent nanomaterials are their incorporation into circularly polarised light emissive devices, which can be used in circular dichroism spectroscopy, chiral asymmetric synthesis <sup>20, 76</sup> and spintronics<sup>77, 78</sup>. To date this has been achieved with the use of achiral QDs in a chiral periodic structure, also known as a chiral photonic crystal, produced through advanced nano-fabrication approaches <sup>79</sup>. These structures have been proposed to possess strong optical activity, due to the use of the gammadion structure, which has no in-plane mirror symmetry but possess a fourfold rotational axis, and on-waveguide planar chiral structures.<sup>80, 81</sup> The first design of this type demonstrated consisted of a chiral photonic crystal of GaAs gammadion layer, specifically a GaAs waveguide-core layer that incorporates an emitter layer containing InAs QDs, and an Al<sub>0.7</sub>Ga<sub>0.3</sub>As clad layer on a GaAs substrate (Fig. 10). PL spectra of the InAs QDs incorporated into this chiral nanostructure differs considerably for left- (ILCP) and right circularly polarized (IRCP) components with strong left-right PL asymmetry observed between 1000 and 1060 nm with a large CD transmission also present in this wavelength region. The PL spectrum of the left- (right-) circularly polarized component from the left-twisted gammadion sample matches that of the right- (left-) circularly polarized component

from the right twisted sample. This shows that the helicity of the emitted light depends on whether the chiral nanostructures are left or right twisted, with the circular polarization



degree (CPD) at maximum reported to be 26%.

**Fig. 10.** (color online). (A) Schematic of designed chiral nanostructure. Gammadion and waveguide-core layers are fabricated of GaAs. Typical scanning electron microscopy image of a chiral photonic crystal with a left twisted gammadion is also shown. Length of white scale bar corresponds to 1  $\mu$ m. Values of the indicated structural parameters are given in the text. (B) Measured ellipticity spectra in the zero-order transmitted light of the chiral photonic crystals. Gray (red) [black (blue)] line indicates the result obtained with the left- [right-] twisted gammadion sample. Reproduced with permission from reference <sup>79</sup>.

Following upon this initial work, CPD of as high as 81% was achieved <sup>82</sup> by fabrication of a chiral gammadion layer structure with partial etching of an upper Bragg mirror and a layer of InAs QDs. This nanostructure consisted of 23.5/20 pairs of AlAs/GaAs layers in the lower/upper Bragg reflectors and a GaAs active layer with an incorporated InAs QD layer, which allowed for the large increase in CPD. Alternatively, a new optimal design for a QD based chiral photonic crystal was also recently proposed in the literature <sup>83</sup> using a computational modelling approach that is claimed to be able to produce a CPD of 99%. This was based upon the very similar design reported in ref <sup>79</sup>, but instead of utilising a gammadion structure, four rectangles are used, each rotated 90° with respect to its nearest neighbour. This structure (Fig. 11) could also potentially prove easier to manufacture as claimed by the authors.

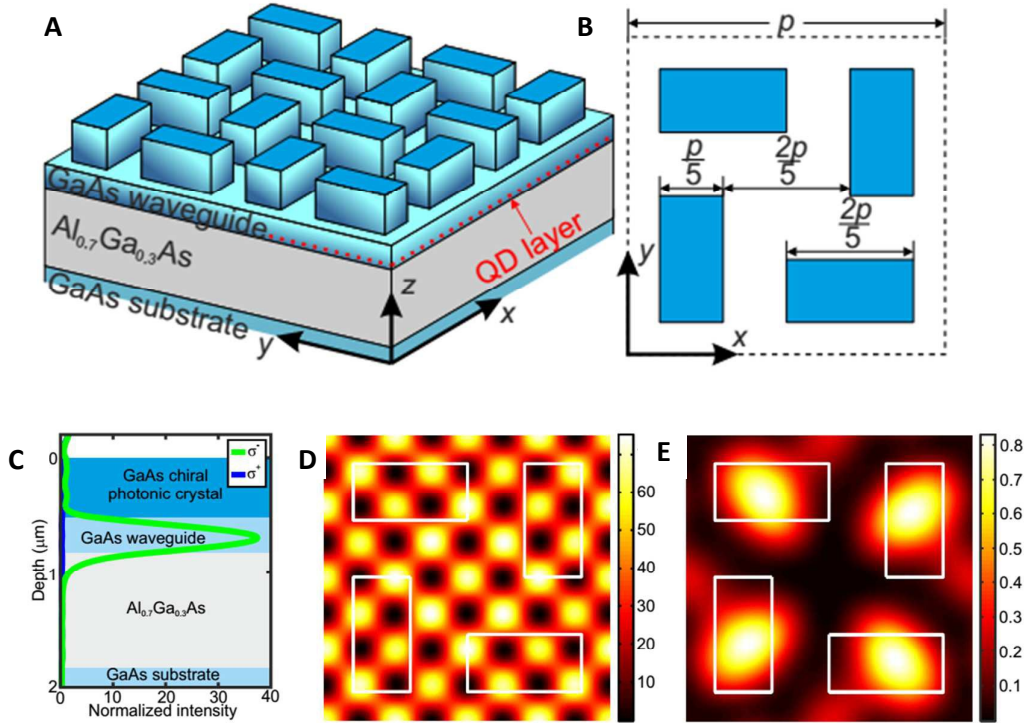


**Fig. 11.** (a) Three-dimensional side view and (b) top view of the optimized chiral nanostructure. (c) Calculated dependencies of left ( $\sigma^-$ ) and right ( $\sigma^+$ ) circularly polarized components of the far-field emission on the vertical position of the layer with randomly distributed QDs. The blue, light blue and gray rectangles mark the chiral photonic crystal layer, GaAs waveguide, and  $\text{Al}_{0.7}\text{Ga}_{0.3}\text{As}$  layer, respectively. (d,e) Calculated dependencies of (d) left and (e) right circularly polarized components of the single QD's far-field emission along  $z$  direction on its horizontal position (depth is 740 nm). One unit cell (period is  $p = 920$  nm) is shown in all pictures. White rectangles mark horizontal positions of chiral photonic crystal elements. Reproduced with permission from referenc<sup>83</sup>.

Another structure, which was proposed as a means to produce circularly polarised emission involves the use of three identical quantum dots in a trigonal formation, also termed a triangular-quantum-dot (TQD). This should show tuneable emission when a magnetic field is applied with orientation perpendicular to the plane, with the three identical quantum dots electronic wave functions acquiring chirality<sup>84</sup>. Each TQD molecule is predicted to exhibit CPL birefringence, which becomes strong above a threshold frequency, at which point the TQD molecule becomes completely transparent to one of the two CPLs. Furthermore, this structure is also proposed as an active medium for CPL lasing action. Another novel CPL emissive structure utilises a U shaped split ring resonator (SRRs), which have been the subject of extensive research in the last 10 years<sup>85-88</sup>. The SRRs act as a multipolar

nanoantenna coupled to a semiconductor QD, showing emission at around 800 nm.<sup>89</sup> This specific SRR is arranged in a periodic lattice, with a lattice constant of 300 nm on a glass substrate and was covered with an MgF<sub>2</sub> spacer. A uniform layer of QDs was then spin-coated on top of the MgF<sub>2</sub> layer; with a thickness of 12 nm so as to achieve the highest coupling efficiency between the QDs and the SRRs. This constructed nanoantenna then demonstrated polarised luminescent emission under optical pumping, producing strong CPL emission, with the degree of polarisation greatly dependent upon direction.

Thus, though none of these structures at present use chiral QDs or metal NCs in their construction, we propose that they could be hugely beneficial when incorporation into these structures, allowing for enhancement of the CPL signals already produced from the materials arrangements and therefore enabling even greater control of the CPL produced.

#### 4.5. Spintronics

A new class of faster, more efficient electronic devices are being investigated at present based upon the emerging field of spintronics (spin transport electronics).<sup>90</sup> In this new type of electronic device, the spin of the electron is used to transfer information and therefore to perform computations, instead of the charge of the electron. For these devices to be possible, spin polarisation is an important characteristic, meaning electrons transported through the medium show a higher population of one spin than of the other. Recently, it has been demonstrated that chiral molecules exhibit large spin polarisation in photoelectrons which has been termed chiral induced spin selectivity<sup>91</sup>. Correspondingly, huge interest has been shown in quantum dots for spintronic applications, due to the long spin coherent times of electrons in these nanostructures<sup>92-94</sup>. Therefore, the combination of chiral QDs should enable unique control of the spin of electrical currents. A recent publication demonstrated the use of a chiral molecule, to transmit excited electrons from a QD which acted as a photoelectron producer<sup>95</sup>. In this setup, a spin torque is shown to be transferred from either CdSe or InAs QDs to a ferromagnetic material through the chiral molecule of  $\alpha$  helix L-polyalanine. This demonstrates the principle application of a photogenerated electrons to induce a local magnetization without the traditional use of an external magnet, and therefore could form the basis for highly localized nanometric spintronic 3D logic devices<sup>95</sup>. To date, no chiral QDs or metal NCs of any type have been tested in this area but could prove an invaluable tool in electron spin control, by eliminating the need for conductive chiral ligands.

## 5. Conclusions and future outlook

From the review above we can witness the fast-growing interest in chiral quantum nanostructures and the significant development of this field over the last few years.

Reports of the induction of chirality in CdSe based quantum dot structures by a simple chiral ligand assisted phase transfer of initially non-chiral QDs<sup>18, 19</sup> are very important and open up new approaches in the development of chiral nanomaterials. It is expected that such convenient methods to induce chirality will be extensively used for the preparation of chiral semiconducting and potentially other inorganic chiral nanostructures in the near future. In addition; the demonstration of circular polarised light emission by QDs with induced chirality might find a range of potential applications in various optical devices, components of chiroptical detectors, polarimeters, CD spectrometers and in the long term even in colour displays. In overall; very significant advancements in the development of real applications for chiral QDs have been demonstrated during the last 2 years. These include sensing of various chiral organic drug molecules<sup>49</sup> and catalysis of asymmetric aldol condensation reactions.<sup>73</sup> Both these applications are very important and should attract more interest in chiral QD based nanomaterials.

In addition, over the last years there have been significant achievements in the development of completely novel types of chiral hybrid nanostructures containing plasmonic and combinations of other nanomaterials in one system. Particularly the development of a new fabrication process which involves a combination of low-temperature shadow deposition with nanoscale patterning that provides access to highly unusually shaped 3D chiral nanomaterials containing multiple components from various materials.<sup>96</sup> Again; this technique can be easily scaled up to produce these nanomaterials in large scale if necessary. Potentially new chiral multicomponent nanomaterials can find many important applications ranging from sensing to catalysis and enantiomeric separation.

A very interesting development is the discovery of intrinsic chirality of CdSe/ZnS quantum dots and rods stabilized by achiral ligands<sup>21</sup> and CdTe QDs capped with achiral ligands,<sup>20</sup> as well as a novel approach for the separation of chiral nanostructures from their racemic mixtures by a chiral ligand assisted phase transfer process. We expect that this approach will open up new exciting possibilities in separation and investigation of various chiral nano-sized objects and may find a number of technologically important applications. The experimental

observation of intrinsic chirality QDs stabilised by achiral ligands is also of immense importance. In this case QDs which are prepared by a conventional hot injection method (without using any chiral ligands) are in fact produced as a racemic mixture of enantiomeric D- and L-nanocrystals which are formed in tandem with a population of non-chiral nanoparticles. The chirality of these QDs is caused by the presence of chiral defects such as left- and right- handed screw dislocations and potentially some other defects.<sup>21</sup> We believe that not only II-VI semiconducting nanocrystals but also many other colloidal inorganic nanoparticulate systems have a similar intrinsic chiral nature. Since chirality plays a crucial effect in chemical recognition and interactions between chemical and biological species, these findings are expected to produce pronounced effect on nano-bio-technology research and may lead even to some revision of existing approaches in the crucial areas such as nanotoxicology and the application of nanoparticles to medical diagnostics and drug delivery. In general, we expect that further uses for chiral nanomaterials will continue to develop rapidly and the demand for these materials will grow in the near future. However, further detailed systematic experimental and theoretical studies will be needed for fundamental understanding of the properties and behaviour of these new chiral nanostructures for the development of appropriate applications.

### Acknowledgments

The authors acknowledge financial support from Science Foundation Ireland (Grants SFI 12/IA/1300), FP7 FutureNanoNeeds grant and the Ministry of Education and Science of the Russian Federation (Grant no. 14.B25.31.0002).

### References

1. A. O. Govorov, Y. K. Gun'ko, J. M. Slocik, V. A. Gerard, Z. Y. Fan and R. R. Naik, *Journal of Materials Chemistry*, 2011, **21**, 16806-16818.
2. A. Guerrero-Martinez, J. Lorenzo Alonso-Gomez, B. Auguie, M. Magdalena Cid and L. M. Liz-Marzan, *Nano Today*, 2011, **6**, 381-400.
3. M. P. Moloney, Y. K. Gun'ko and J. M. Kelly, *Chemical Communications*, 2007, 3900-3902.
4. S. D. Elliott, M. P. Moloney and Y. K. Gun'ko, *Nano Letters*, 2008, **8**, 2452-2457.
5. J. E. Govan, E. Jan, A. Querejeta, N. A. Kotov and Y. K. Gun'ko, *Chemical Communications*, 2010, **46**, 6072-6074.
6. A. Ben-Moshe, B. M. Maoz, A. O. Govorov and G. Markovich, *Chemical Society Reviews*, 2013, **42**, 7028-7041.
7. Y. Wang, J. Xu, Y. Wang and H. Chen, *Chemical Society Reviews*, 2013, **42**, 2930-2962.
8. J. Wang, S. Liu, C. Zhang, H. Xu and X. Yang, *Progress in Chemistry*, 2011, **23**, 669-678.
9. H. Liu, X. Shen, Z.-G. Wang, A. Kuzyk and B. Ding, *Nanoscale*, 2014, **6**, 9331-9338.
10. S. A. Gallagher, M. P. Moloney, M. Wojdyla, S. J. Quinn, J. M. Kelly and Y. K. Gun'ko, *Journal of Materials Chemistry*, 2010, **20**, 8350-8355.

11. M. Wojdyla, S. A. Gallagher, M. P. Moloney, Y. K. Gun'ko, J. M. Kelly, L. M. Magno, S. J. Quinn, I. P. Clark, G. M. Greetham and M. Towrie, *Journal of Physical Chemistry C*, 2012, **116**, 16226-16232.
12. M. P. Moloney, S. A. Gallagher and Y. K. Gun'ko, *MRS Online Proceedings Library*, 2009, **1241**, null-null.
13. V. A. Gerard, M. Freeley, E. Defrancq, A. V. Fedorov and Y. K. Gun'ko, *Journal of Nanomaterials*, 2013.
14. M. P. Moloney, J. Govan, A. Loudon, M. Mukhina and Y. K. Gun'ko, *Nature Protocols*, 2015, **10**, 558-573.
15. Y. Xia, Y. Zhou and Z. Tang, *Nanoscale*, 2011, **3**, 1374-1382.
16. T. Nakashima, Y. Kobayashi and T. Kawai, *Journal of the American Chemical Society*, 2009, **131**, 10342-+.
17. Y. Zhou, M. Yang, K. Sun, Z. Tang and N. A. Kotov, *Journal of the American Chemical Society*, 2010, **132**, 6006-6013.
18. U. Tohgha, K. K. Deol, A. G. Porter, S. G. Bartko, J. K. Choi, B. M. Leonard, K. Varga, J. Kubelka, G. Muller and M. Balaz, *ACS Nano*, 2013, **7**, 11094-11102.
19. U. Tohgha, K. Varga and M. Balaz, *Chemical Communications*, 2013, **49**, 1844-1846.
20. J. Yeom, B. Yeom, H. Chan, K. W. Smith, S. Dominguez-Medina, J. H. Bahng, G. P. Zhao, W. S. Chang, S. J. Chang, A. Chuvilin, D. Melnikau, A. L. Rogach, P. J. Zhang, S. Link, P. Kral and N. A. Kotov, *Nature Materials*, 2015, **14**, 66-72.
21. M. V. Mukhina, V. G. Maslov, A. V. Baranov, A. V. Fedorov, A. O. Orlova, F. Purcell-Milton, J. Govan and Y. K. Gun'ko, *Nano Letters*, 2015, **15**, 2844-2851.
22. M. V. M. Mukhina, V. G.; Korsakov, I. V.; Purcell Milton, F.; Loudon, A.; Baranov, A. V.; Fedorov, A. V. & Gun'ko, Y. K, *MRS Proc.*, 2015, **1793**, mrs15-2125910.
23. A. Ben-Moshe, A. O. Govorov and G. Markovich, *Angewandte Chemie-International Edition*, 2013, **52**, 1275-1279.
24. A. S. Baimuratov, I. D. Rukhlenko, Y. K. Gun'ko, A. V. Baranov and A. V. Fedorov, *Nano Letters*, 2015, **15**, 1710-1715.
25. A. S. Baimuratov, I. D. Rukhlenko, R. E. Noskov, P. Ginzburg, Y. K. Gun'ko, A. V. Baranov and A. V. Fedorov, *Scientific Reports*, 2015, **5**, 14712-14712.
26. P. D. Jadzinsky, G. Calero, C. J. Ackerson, D. A. Bushnell and R. D. Kornberg, *Science*, 2007, **318**, 430-433.
27. H. Qian, W. T. Eckenhoff, Y. Zhu, T. Pintauer and R. Jin, *Journal of the American Chemical Society*, 2010, **132**, 8280-8281.
28. I. Dolamic, S. Knoppe, A. Dass and T. Buerger, *Nature Communications*, 2012, **3**.
29. S. Knoppe, O. A. Wong, S. Malola, H. Hakkinen, T. Buerger, T. Verbiest and C. J. Ackerson, *Journal of the American Chemical Society*, 2014, **136**, 4129-4132.
30. S. Knoppe, A. C. Dharmaratne, E. Schreiner, A. Dass and T. Buerger, *Journal of the American Chemical Society*, 2010, **132**, 16783-16789.
31. C. Zeng, T. Li, A. Das, N. L. Rosi and R. Jin, *Journal of the American Chemical Society*, 2013, **135**, 10011-10013.
32. C. Zeng, Y. Chen, K. Kirschbaum, K. Appavoo, M. Y. Sfeir and R. Jin, *Science Advances*, 2015, **1**.
33. L. B. Zhang and E. K. Wang, *Nano Today*, 2014, **9**, 132-157.
34. P. Alivisatos, *Nature Biotechnology*, 2004, **22**, 47-52.
35. L. F. Shi, V. De Paoli, N. Rosenzweig and Z. Rosenzweig, *Journal of the American Chemical Society*, 2006, **128**, 10378-10379.
36. R. C. Somers, M. G. Bawendi and D. G. Nocera, *Chemical Society Reviews*, 2007, **36**, 579-591.
37. L. Basabe-Desmonts, D. N. Reinhoudt and M. Crego-Calama, *Chemical Society Reviews*, 2007, **36**, 993-1017.
38. G. Konstantatos and E. H. Sargent, *Nature Nanotechnology*, 2010, **5**, 391-400.
39. V. Biju, Y. Makita, A. Sonoda, H. Yokoyama, Y. Baba and M. Ishikawa, *Journal of Physical Chemistry B*, 2005, **109**, 13899-13905.

40. P. T. Snee, R. C. Somers, G. Nair, J. P. Zimmer, M. G. Bawendi and D. G. Nocera, *Journal of the American Chemical Society*, 2006, **128**, 13320-13321.
41. C. P. Han and H. B. Li, *Small*, 2008, **4**, 1344-1350.
42. Y. Wei, H. Li, H. Hao, Y. Chen, C. Dong and G. Wang, *Polymer Chemistry*, 2015, **6**, 591-598.
43. Y. Wei, H. Hao, J. Zhang, X. Hao and C. Dong, *Analytical Methods*, 2014, **6**, 3227-3230.
44. C. Carrillo-Carrion, S. Cardenas, B. M. Simonet and M. Valcarcel, *Analytical Chemistry*, 2009, **81**, 4730-4733.
45. T. Delgado-Perez, L. M. Bouchet, M. de la Guardia, R. E. Galian and J. Perez-Prieto, *Chemistry-a European Journal*, 2013, **19**, 11068-11076.
46. W. Tedsana, T. Tuntulani and W. Ngeontae, *Analytica Chimica Acta*, 2015, **867**, 1-8.
47. T. Liu, Y. Y. Su, H. J. Song and Y. Lv, *Analyst*, 2013, **138**, 6558-6564.
48. L. Song, S. Wang, N. A. Kotov and Y. Xia, *Analytical Chemistry*, 2012, **84**, 7330-7335.
49. T. Delgado-Pérez, L. M. Bouchet, M. de la Guardia, R. E. Galian and J. Pérez-Prieto, *Chemistry – A European Journal*, 2013, **19**, 11068-11076.
50. C. Buzea, Pacheco, II and K. Robbie, *Biointerphases*, 2007, **2**, MR17-MR71.
51. K. Pulskamp, S. Diabate and H. F. Krug, *Toxicology Letters*, 2007, **168**, 58-74.
52. M. Heinlaan, A. Ivask, I. Blinova, H. C. Dubourguier and A. Kahru, *Chemosphere*, 2008, **71**, 1308-1316.
53. H. F. Krug and P. Wick, *Angewandte Chemie-International Edition*, 2011, **50**, 1260-1278.
54. Y. Li, Y. Zhou, H.-Y. Wang, S. Perrett, Y. Zhao, Z. Tang and G. Nie, *Angewandte Chemie International Edition*, 2011, **50**, 5860-5864.
55. C. L. Zhang, K. Wang, C. Li, Y. L. Liu, H. L. Fu, F. Pan and D. X. Cui, *Journal of Materials Chemistry B*, 2014, **2**, 6931-6938.
56. C. L. Zhang, Z. J. Zhou, X. Zhi, Y. Ma, K. Wang, Y. X. Wang, Y. G. Zhang, H. L. Fu, W. L. Jin, F. Pan and D. X. Cui, *Theranostics*, 2015, **5**, 134-149.
57. X. Michalet, F. F. Pinaud, L. A. Bentolila, J. M. Tsay, S. Doose, J. J. Li, G. Sundaresan, A. M. Wu, S. S. Gambhir and S. Weiss, *Science*, 2005, **307**, 538-544.
58. A. M. Smith, H. Duan, A. M. Mohs and S. Nie, *Advanced Drug Delivery Reviews*, 2008, **60**, 1226-1240.
59. X. Wu, X. X. He, K. M. Wang, C. Xie, B. Zhou and Z. H. Qing, *Nanoscale*, 2010, **2**, 2244-2249.
60. M. A. H. Muhammed, P. K. Verma, S. K. Pal, R. C. A. Kumar, S. Paul, R. V. Omkumar and T. Pradeep, *Chemistry-a European Journal*, 2009, **15**, 10110-10120.
61. X. Yang, L. F. Gan, L. Han, D. Li, J. Wang and E. K. Wang, *Chemical Communications*, 2013, **49**, 2302-2304.
62. Y. Wang and A. M. Chen, *Organic Process Research & Development*, 2008, **12**, 282-290.
63. D. H. Dressler and Y. Mastai, *Chirality*, 2007, **19**, 358-365.
64. A. Kamal, M. A. Azhar, T. Krishnaji, M. S. Malik and S. Azeza, *Coordination Chemistry Reviews*, 2008, **252**, 569-592.
65. Y. Okamoto and E. Yashima, *Angewandte Chemie-International Edition*, 1998, **37**, 1020-1043.
66. H. S. Wang and J. P. Wei, *Nanoscale*, 2015, **7**, 11815-11832.
67. A. Zecchina, E. Groppo and S. Bordiga, *Chemistry – A European Journal*, 2007, **13**, 2440-2460.
68. P. Barbaro, V. D. Santo and F. Liguori, *Dalton Transactions*, 2010, **39**, 8391-8402.
69. S. Jansat, D. Picurelli, K. Pelzer, K. Philippot, M. Gomez, G. Muller, P. Lecante and B. Chaudret, *New Journal of Chemistry*, 2006, **30**, 115-122.
70. M. L. Kantam, T. Ramani, L. Chakrapani and K. V. Kumar, *Tetrahedron Letters*, 2008, **49**, 1498-1501.
71. S. Wang, R. Li, C. Zhang, Y. Li, B. Li and Y. Yang, *Materials Letters*, 2013, **106**, 71-74.
72. C. Chen, H. Shi and G. Zhao, *The Journal of Physical Chemistry C*, 2014, **118**, 12041-12049.
73. E. Shah and H. P. Soni, *RSC Advances*, 2013, **3**, 17453-17461.
74. I. Sato, K. Kadowaki, H. Urabe, J. H. Jung, Y. Ono, S. Shinkai and K. Soai, *Tetrahedron Letters*, 2003, **44**, 721-724.

75. T. Kawasaki, Y. Araki, K. Hatase, K. Suzuki, A. Matsumoto, T. Yokoi, Y. Kubota, T. Tatsumi and K. Soai, *Chemical Communications*, 2015, **51**, 8742-8744.
76. J. Kim, J. Lee, W. Y. Kim, H. Kim, S. Lee, H. C. Lee, Y. S. Lee, M. Seo and S. Y. Kim, *Nat Commun*, 2015, **6**.
77. P. Nemeč, E. Rozkotová, N. Tesařová, F. Trojanek, E. De Ranieri, K. Olejník, J. Zemen, V. Novak, M. Cukr, P. Maly and T. Jungwirth, *Nature Physics*, 2012, **8**, 411-415.
78. T. Yokoyama and S. Murakami, *Physica E-Low-Dimensional Systems & Nanostructures*, 2014, **55**, 1-8.
79. K. Konishi, M. Nomura, N. Kumagai, S. Iwamoto, Y. Arakawa and M. Kuwata-Gonokami, *Physical Review Letters*, 2011, **106**, 4.
80. B. Bai, Y. Svirko, J. Turunen and T. Vallius, *Physical Review A*, 2007, **76**, 12.
81. B. F. Bai, K. Konishi, X. F. Meng, P. Karvinen, A. Lehmuskero, M. Kuwata-Gonokami, Y. Svirko and J. Turunen, *Optics Express*, 2009, **17**, 688-696.
82. A. A. Maksimov, Tartakovskii, II, E. V. Filatov, S. V. Lobanov, N. A. Gippius, S. G. Tikhodeev, C. Schneider, M. Kamp, S. Maier, S. Hofling and V. D. Kulakovskii, *Physical Review B*, 2014, **89**, 5.
83. S. V. Lobanov, T. Weiss, N. A. Gippius, S. G. Tikhodeev, V. D. Kulakovskii, K. Konishi and M. Kuwata-Gonokami, *Optics Letters*, 2015, **40**, 1528-1531.
84. P. Kotetes, P. Q. Jin, M. Marthaler and G. Schon, *Physical Review Letters*, 2014, **113**, 5.
85. F. Aznar, M. Gil, J. Bonache and F. Martin, *Opto-Electronics Review*, 2008, **16**, 226-236.
86. M. Duran-Sindreu, J. Naqui, J. Bonache and F. Martin, *International Journal of Rf and Microwave Computer-Aided Engineering*, 2012, **22**, 439-458.
87. F. Martin and J. Bonache, *Sensors*, 2014, **14**, 22848-22863.
88. F. Monticone and A. Alu, *Journal of Materials Chemistry C*, 2014, **2**, 9059-9072.
89. S. S. Kruk, M. Decker, I. Staude, S. Schlecht, M. Greppmair, D. N. Neshev and Y. S. Kivshar, *ACS Photonics*, 2014, **1**, 1218-1223.
90. S. A. Wolf, D. D. Awschalom, R. A. Buhrman, J. M. Daughton, S. von Molnar, M. L. Roukes, A. Y. Chtchelkanova and D. M. Treger, *Science*, 2001, **294**, 1488-1495.
91. R. Naaman and D. H. Waldeck, *Annual Review of Physical Chemistry, Vol 66*, 2015, **66**, 263-281.
92. D. D. Awschalom and M. E. Flatte, *Nat Phys*, 2007, **3**, 153-159.
93. L. Bogani and W. Wernsdorfer, *Nat Mater*, 2008, **7**, 179-186.
94. R. J. Warburton, *Nat Mater*, 2013, **12**, 483-493.
95. O. Ben Dor, N. Morali, S. Yochelis, L. T. Baczewski and Y. Paltiel, *Nano Letters*, 2014, **14**, 6042-6049.
96. A. G. Mark, J. G. Gibbs, T.-C. Lee and P. Fischer, *Nat Mater*, 2013, **12**, 802-807.